Advanced Composites and Hybrid Materials (2021) 4:957–965
https://doi.org/10.1007/s42114-021-00263-8

ORIGINAL RESEARCH

Shape memory polymer solar cells with active deformation

Hui Gao[1] · Jinrong Li[1] · Yanju Liu[2] · Jinsong Leng[1]

Received: 10 February 2021 / Revised: 21 April 2021 / Accepted: 29 April 2021 / Published online: 9 June 2021
© The Author(s), under exclusive licence to Springer Nature Switzerland AG 2021

Abstract
The reliable and lightweight deployable solar arrays require the capability of large deformation for packaging and the ability to actively deform for deployment. To satisfy such demands, the shape memory polymer solar cells (SMPSCs) are fabricated and demonstrated in this paper by using flexible and conductive silver nanowire/shape memory copolyamide (AgNW/SMPI) composite film as the transparent substrates. The AgNW/SMPI composite film has good optical transparency (~73% at the wavelength of 450 ~ 1100 nm), smooth surfaces (average RMS: ~3.32 nm), good shape memory performances (shape fixation ratio > 98%, shape recovery ratio > 98%), and can maintain excellent conductivity (~10Ω/□) after mechanical deformations with large strain. Owing to the shape memory effect of the substrate, SMPSCs can be deformed into arbitrary shape and actively recover to the original shape upon heating. The power conversion efficiency of SMPSC (2.94%) is lower than that of ITO-based solar cells with the same structure (3.44%), due to the relatively lower optical transparency of SMPI. However, SMPSCs can maintain good photovoltaic performances after 50 bending-recovery cycles or few shape recovery cycles, demonstrating better flexibility and durability than ITO-based solar cells. The SMPSCs have the potential to be used in deployable solar arrays, and the transparent conductive SMPI film electrodes have the potential to be used in areas of sensors, medical probes, and displays.

Keywords Shape memory electrode · Flexible solar cells · Active shape changing · Durability · Shape memory copolyamide

1 Introduction

Deployable solar arrays are vital components for spacecraft. Most of the current deployable solar arrays have complicated structures and utilize non-controllable, non-testable, and non-reusable electro-explosive devices for deployment, which may lead to high impact and the risk of malfunction. To fabricate reliable and lightweight ultra-large deployable solar arrays with simple structures, the capability of large deformation for packaging to save the space before launching and the ability to actively deform for deployment will be required. Shape memory polymers (SMPs) are typical smart polymers that can response to external stimuli [1–14] and demonstrate huge application potential in the field of deployable aerospace structures [1]. SMP structure can be deformed from original shape into complex shape due to the low modulus of SMPs at temperature higher than the transition temperature. After cooling, the stiffness of SMPs increases significantly, and such complex shape can be fixed. When being heated again, the structure can actively recover from different pre-deformed shapes to the original shape. Owing to the above features, SMPs are suitable for the substrate of deployable solar arrays. In reports, shape memory function has been endowed with some flexible electronic devices when employing shape memory polymers (SMPs) as substrates [13–16]. Accordingly, the flexible solar cells with shape memory properties are feasible.

Since SMPs are not conductive, the electrode material is a challenge for fabricating the shape memory solar cells. Although extensively utilized as the electrode in electronic devices [17–20], indium tin oxide (ITO) cannot satisfy the requirements of large deformation due to its intrinsic brittleness. Even coated on a polymer film, ITO still breaks easily at relatively low bending strain or under repeated bending-recovery cycles, which results in severe deterioration

✉ Jinsong Leng
lengjs@hit.edu.cn

[1] Center for Composite Materials and Structures, Harbin Institute of Technology, Harbin 150080, Heilongjiang, China

[2] Department of Astronautical Science and Mechanics, Harbin Institute of Technology, Harbin 150001, Heilongjiang, China

in electrical conductivity [21]. Novel electrode materials have been developed to improve the flexibility of electronic devices [22–37], including graphene [22–24], carbon nanotubes [25–27], metal grids [28–30], random metal nanowires [16, 21, 31, 32], conducting polymers [33], and their combinations [34–36]. Among these electrode materials, silver nanowires (AgNWs), fabricated by drop-casting [16, 34, 38], Meyer rod coating [39, 40], spray coating [41, 42], or vacuum filtering [43] are promising due to their low resistivity and high optical transparency. Moreover, the AgNWs could remain conductive while bending. However, the uneven surface may lead to shorts across the functional layers, and the poor adhesion to the substrates makes AgNW electrodes unsuitable for direct employment in flexible electronics [38, 40]. The adhesion to polymers and the surface quality of the AgNWs can be effectively improved through embedding AgNWs into polymers [44, 45]. These composite electrodes have good conductivity and optical transparency, low surface roughness, and low conductivity reduction after mechanical deformation [44, 45] and have been utilized in some flexible electronic devices like solar cells and light-emitting diodes [16, 32, 37].

In this paper, we demonstrate the shape memory polymer solar cells (SMPSCs) which utilize the transparent and conductive AgNW/shape memory polyimide (SMPI) composite as the substrates and electrodes. The transparent SMPI is chosen as the substrate because it has application potential in the field of aerospace and flexible electronics due to its excellent mechanical strength, good optical transparency, high-temperature and radiation resistance, light weight, chemical inertness, and low thermal expansion coefficient [2, 3, 46–48]. The glass transition temperature (T_g) of the SMPI used in this work is 182 ℃, and other basic properties of the SMPI film are listed in Table 1 and shown in the Supporting Information. The transparent electrodes were fabricated through embedding AgNW into synthesized SMPI substrates using a simple and low-cost fabrication method. The AgNW/SMPI electrodes could remain good optical transparency and conductivity after bending-recovery cycles. Due to the shape memory effect of the AgNW/SMPI electrode, SMPSCs can be deformed into arbitrary shape and recover to the original shape upon heating. The SMPSCs demonstrate better flexibility and durability than ITO/glass-based solar cells, while the power conversion efficiency (PCE) of the SMPSCs is just slightly lower than that of ITO/glass-based solar cells.

2 Experimental section

2.1 Materials

Poly(3-hexylthiophene) (P3HT, 99.99%), phenyl-C61-butyric acid methyl ester (PC61BM, 99.99%), and bisphenol A dianhydride (BPADA, 97%) were obtained from Sigma-Aldrich Co. LLC. (USA). 1,3-bis(3-aminophenoxy)benzene (BAB, 98%) was achieved from Tokyo Chemical Industry Co., Ltd. (TCI, Japan). Lithium fluoride (LiF), aluminum (Al), and 4,4′-(1,1′-Biphenyl-4,4′-diyldioxy)dianiline (BAPB, 97%) were bought from Aladdin Bio-Chem Technology Co., Ltd. (Shanghai, China). Dimethylacetamide (DMAc) was purchased from Kemiou Chemical Reagent Co., Ltd. (Tianjin, China) and distilled with activated 4 Å molecular sieves for 24 h under reduced pressure. Poly(3,4-ethylenedioxythiophene):poly(styrenesulfonate) (PEDOT:PSS, Clevios P VP AI4083) were purchased from Heraeus Materials Technology Shanghai Ltd. (China). ITO/glass and ITO/PEN with the sheet resistance of ~9 Ω/□ and ~35 Ω/□ was afforded by Yingkou You Xuan Trade Co., Ltd. (Liaoning, China). Silver nanowires (average diameter: ~70 nm, average length: ~40 μm) were provided by Seashell Tech. (California, USA).

2.2 Fabrication of shape memory silver nanowire/polymer composite electrodes

The fabrication processes of shape memory AgNW/SMPI composite electrodes are schematically shown in Fig. S1. Before the spin-coating of AgNW solution, the glass substrate was ultrasonically cleaned in detergent, deionized water, acetone, ethanol, and isopropanol in turn. AgNW solution, which has been diluted to the required concentration with isopropyl alcohol, was spin-coated onto glass substrates at 500 rpm for 9 s and then 1100 rpm for 30 s. After drying the AgNW/glass substrates at 80 °C for 30 min, the pre-prepared poly(amic acid) solution (precursor of SMPI, details in Supporting Information) was drop-coated onto

Table 1 Performances comparison of the substrates for devices

Substrates	Thickness (mm)	R_s (Ω/□)	RMS (nm)	Transmittance at 450 ~ 1100 nm (%)	Shape fixity ratio (R_f) (%)	Shape recovery ratio (R_r) (%)
ITO/glass	~1.10	~9	< 10	> 86	–	–
SMPI	~0.120	–	–	> 86	98.8	100
AgNW/SMPI	~0.125	~10	3.32	> 73	98.7	100
AgNW/SMPI	~0.125	~1	1.28	> 35	98.8	100

AgNW and then experienced step-wised curing processes of which the temperature was successively kept at 80 °C, 120 °C, 180 °C, 210 °C, and 250 °C, and each temperature was kept for 2 h. The smooth and flexible shape memory AgNW/SMPI composite electrode was achieved after being peeled off glass substrates in hot deionized water. The thickness of the AgNW/SMPI composite electrodes is determined by the amount of PAA solution and was controlled at around 120 μm in this work.

2.3 Preparation of shape memory polymer solar cells

Before the fabrication of SMPSCs, AgNW/SMPI composite electrodes were ultrasonically cleaned successively in detergent, deionized water, acetone, ethanol, and isopropanol, and then thermally treated at 120 °C for 1 h on vacuum dry chamber. After pre-ultrasonicated for 30 min, PEDOT:PSS solution, without any dilution, was spin-coated onto electrodes at 650 rpm for 9 s and then 3500 rpm for 60 s, and subsequently annealed at 120 °C for 20 min. The thickness of PEDOT:PSS film, measured by a Dektak 6 M stylus profilometer, was around 40 nm. The electrode/PEDOT:PSS was then transferred into a nitrogen-filled glove box where the oxygen and moisture levels are below 1 ppm. Before spin-coating active layer, P3HT and PC61BM, which were mixed in a weight ratio of 1:1, were co-dissolved in 1,2-dichlorobenzene and stirred at 60 °C for 24 h inside the glove box. The P3HT:PC61BM solution (22 mg mL^{-1}) was then spin-coated on the electrode/PEDOT:PSS at 550 rpm for 9 s and then 1100 rpm for 30 s to form a 210-nm-thick film and subsequently annealed at 135 °C for 5 min. A 1-nm-thick LiF thin film and a 100-nm-thick Al electrode were then consecutively thermally evaporated on electrode/PEDOT:PSS/P3HT:PCBM to obtain the SMPSCs. The active area of the SMPSCs was 12 mm^2 which is determined by the shadow mask. Lastly, the whole device was thermally annealed at 120 °C on hot plate for 30 min under nitrogen atmosphere to improve the performances of solar cells. The solar cells with the same structure except for the ITO/glass electrodes were also fabricated as the control devices.

2.4 Performance testing

Ultraviolet–visible (UV–Vis) transmittance of 120-μm-thick SMPI film and AgNW/SMPI composite electrode at the wavelength from 200 to 2000 nm was tested on a Perkin-Elmer Lambda 950 spectrometer, respectively. The sheet resistance (R_s) of the films was tested by a four-probe sheet resistance/resistivity tester (RG-7C, NAPSON). The root-mean-square (RMS) roughness was scanned by an atomic force microscope (AFM, Digital Instrument, NS4/D3100CL, Germany) with the scanning area of 10×10 μm^2 and was analyzed with Nanoscope 1.50 software. The surface images of samples were taken from Quanta 200FEG-scanning electron microscopy (SEM) at an acceleration voltage of 15.0 kV. The photovoltaic performances of solar cells were characterized under a 1.5 solar illumination at 1000 W m^{-2} (1 sun). The current–voltage (*J*-*V*) characteristics of solar cells can be monitored and recorded by computer, from which the open-circuit voltage (V_{oc}) and short-circuit current density (J_{sc}) can be directly read. Fill factor (FF) and PCE can be calculated by the Eqs. S5 and S6 according to Fig. S5, respectively.

3 Results and discussions

3.1 Properties of the AgNW/SMPI composite electrodes

The fabrication process of the shape memory AgNW/SMPI composite electrodes is illustrated in Fig. S1 and detailed in Sect. 2.

The SEM and AFM images of the AgNW/SMPI composite electrodes are shown in Fig. 1a–f. From the SEM images, we can clearly see that AgNWs were uniformly distributed and embedded in the SMPI substrate to form the conductive pathway. The RMS roughness of the shape memory AgNW/SMPI composite electrode with ~10 Ω/□ and ~1 Ω/□ were 3.32 nm and 1.28 nm, respectively, which are comparable to that of ITO (~9 Ω/□, < 10 nm). However, the RMS roughness of the conductive AgNW networks that were directly spin-coated onto SMPI substrates was greater than 100 nm. This is consistent with other reported results [32, 34, 38, 40]. Embedding AgNW into SMPI film can effectively improve the surface quality of the composite electrodes since SMPI will fill out the void inside AgNW networks, which is beneficial to improve the photovoltaic performances of solar cells.

The AgNW/SMPI composite electrodes had high conductivity and optical transparency. The sheet resistance (R_s) of AgNW/SMPI composite electrodes was dependent on the concentration of the AgNW solution and R_s values of about 100 Ω/□, 10 Ω/□, and 1 Ω/□ could be obtained when the concentration is respectively 1.5 mg/mL, 4 mg/mL, and 10 mg/mL. Figure 2a illustrates the UV–Vis transmittance at different wavelength of the AgNW/SMPI composite electrode with different R_s. The increasing of the conductivity is the result of the increased AgNW density, which could enhance the light scattering. Therefore, as can be seen from Fig. 2a, the optical transparency decreased with the increase of conductivity of AgNW/SMPI composite electrode. The AgNW/SMPI composite can also be used as a heater due to its good electrical conductivity. Figure 2b shows the temperature changes of AgNW/SMPI composite electrodes (R_s: ~10 Ω/□) when the external voltage was applied for 600 s and

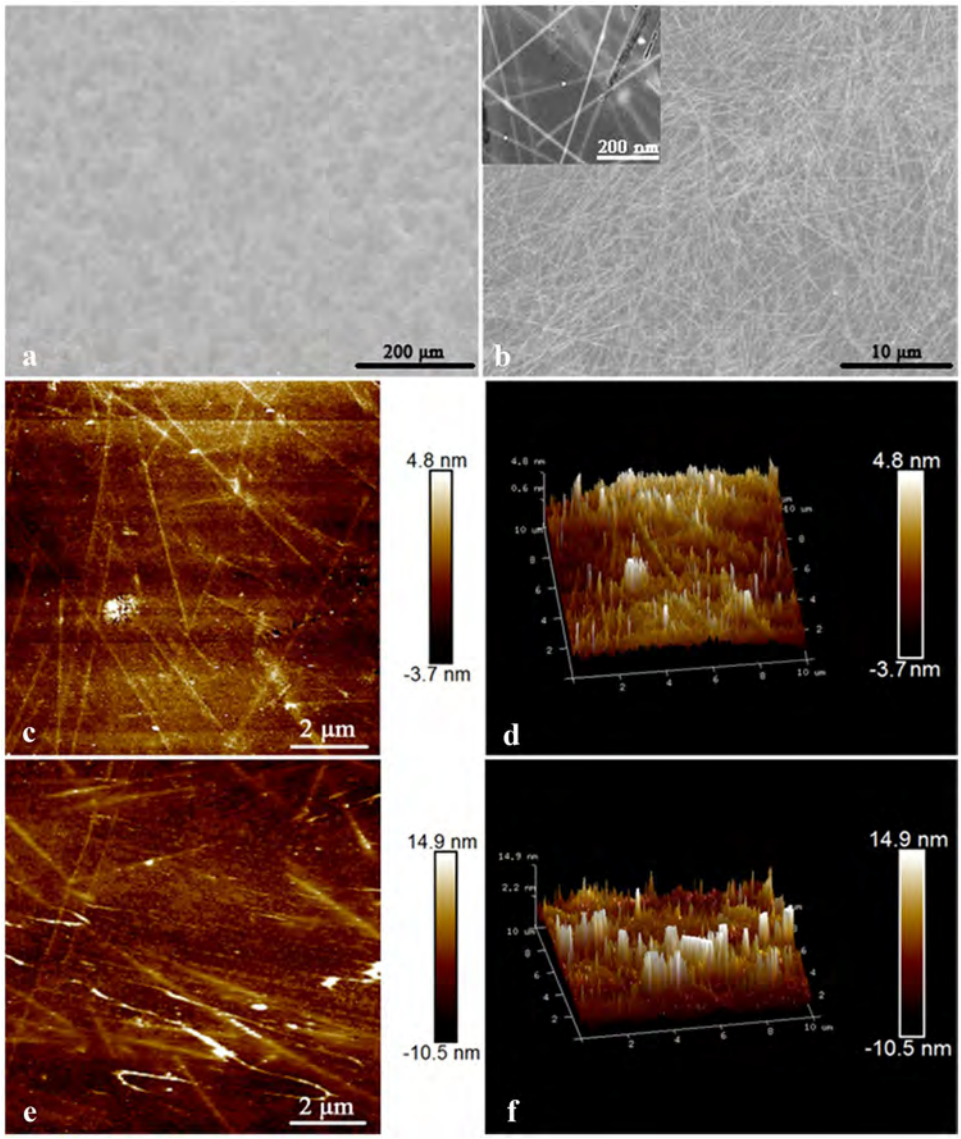

Fig. 1 **a**, **b** SEM morphologies of the AgNW/SMPI composite electrode, showing that AgNW was embedded inside the SMPI substrates. The 2D atomic force microscope (AFM) image (**c**) and 3D AFM image (**d**) of AgNW/SMPI composite electrode with the R_s of ~1 Ω/□. The 2D AFM image (**e**) and 3D AFM image (**f**) of AgNW/SMPI composite electrode with the R_s of ~10 Ω/□

then switched off for another 600 s. That means it is possible to trigger the shape recovery through Joule heating [6].

The AgNW/SMPI composite electrodes also demonstrated excellent flexibility and durability while maintaining high conductivity. We compared the changes in R_s of AgNW/SMPI composite electrode and commonly used ITO/PEN after a number of bending-recovery cycles. The configuration of a rectangular AgNW/SMPI film after bending is illustrated in Fig. S6 (the bending angle is close to 180°), and the results are shown in Fig. 2c. The R_s of ITO/PEN increased by more than one hundred times of its initial value (~35 Ω/□) after only 10 bending-recovery cycles, while the R_s of AgNW/SMPI was almost unchanged after 100 bending-recovery cycles. In addition, the AgNW/SMPI composite electrode had good shape memory performances and could remain good conductivity after 100 bending shape recovery cycles, as shown in Fig. 2d. As shown in Fig. 2e, f, the AgNW/SMPI film could be used as the conductive wire to light the LED when the electrode is in deformed state (bending angle: 90°) and recovered state after 100 shape memory cycles.

Table 1 summarizes the performances of ITO/glass, SMPI, and AgNW/SMPI with R_s of ~10 Ω/□ and ~1 Ω/□. To avoid the decrease of the light absorption of photoactive layers due to low transmittance, the AgNW/SMPI with sheet resistance of ~10 Ω/□ was used in the fabrication of SMPSCs.

3.2 Performance of the shape memory polymer solar cells

The complete layer stack of the SMPSCs is illustrated in Fig. 3a, where PEDOT:PSS, P3HT:PC61BM, LiF served as the hole-transporting layer, active layer, and electron-transporting

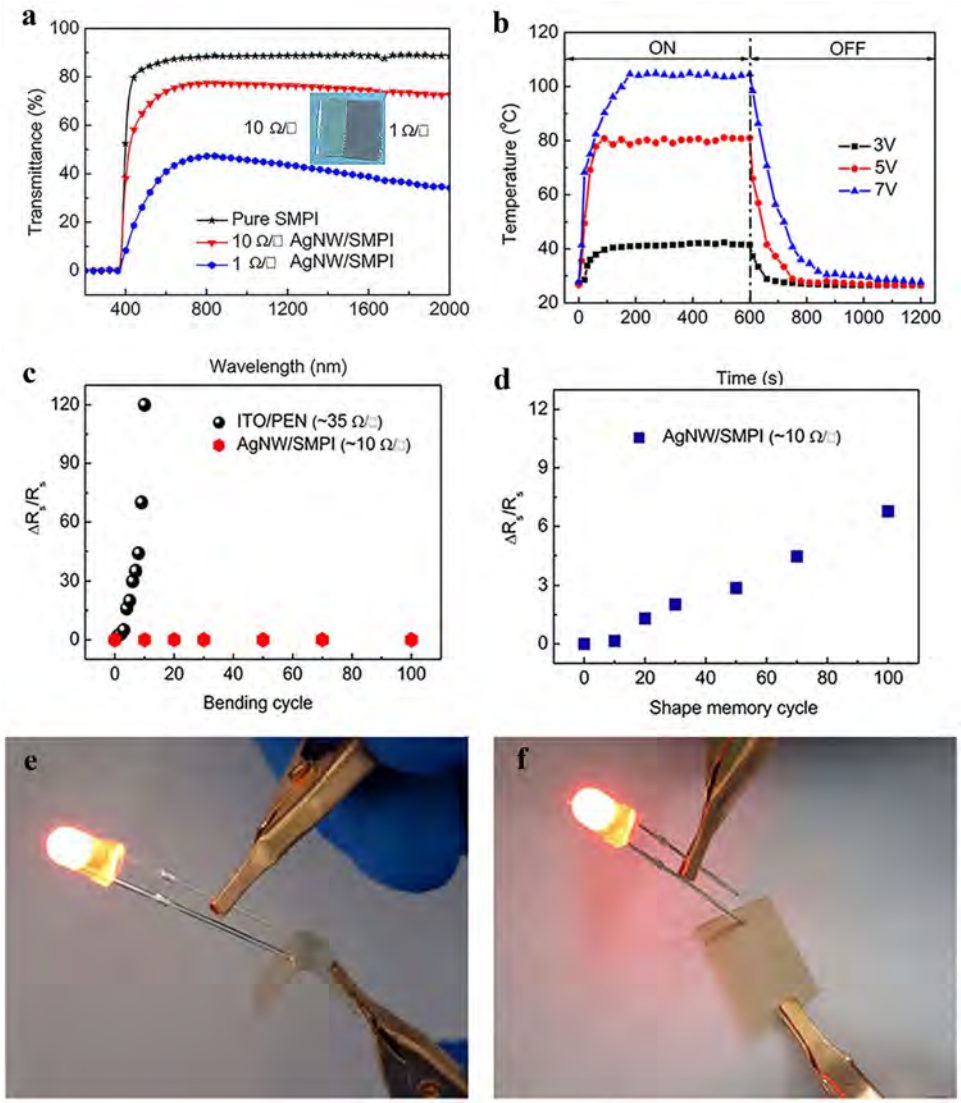

Fig. 2 **a** UV–Vis transmittance spectra of the shape memory AgNW/SMPI composite electrodes with different R_s. **b** The temperature change of AgNW/SMPI composite electrode (R_s: ~10 Ω/□) under different applied voltages. The resistance changes of **c** AgNW/SMPI and ITO/PEN electrodes after bending-recovery cycles and **d** the resistance change of AgNW/SMPI composite electrode after shape memory cycles. The AgNW/SMPI composite electrode was used as the conductive wire to light the LED when the bending angle is 90° (**e**) and 180° (**f**)

layer, respectively, and the band energy diagram for SMPSCs is illustrated in Fig. 3b. The *J-V* characteristics of the solar cells fabricated on ITO (~9 Ω/□) and AgNW composite electrodes (~10 Ω/□) are presented in Fig. 3c, d, respectively. The inset photographs show the solar cells fabricated on ITO electrodes and AgNW/SMPI composite electrodes, respectively. The FF and V_{oc} of two devices were close, and the J_{sc} of solar cells with AgNW electrodes (~7.85 mA/cm^2) was lower than that of solar cells with ITO electrodes (~9.36 mA/cm^2). Correspondingly, the PCE of SMPSCs (2.94%) was lower compared to that of the ITO-based solar cells (3.44%). However, SMPSCs with AgNW/SMPI composite electrodes demonstrated comparable photovoltaic performance to some reported solar cells with AgNW electrode [32, 37]. One possible reason is that the lower optical transparency of AgNW/SMPI electrodes (~73% at wavelength of 450 ~ 1100 nm) than that of ITO electrodes (~88% at wavelength of 450 ~ 1100 nm) reduces the light adsorption of the P3HT:PC61BM and thus leads to the decrease of electron–hole pairs. This can be validated by the rough estimation that the J_{sc} of the solar cell is in proportion to the transmittance of the electrode, since the solar cells we compared had the same structure except for the electrode. The SMPI is chosen in consideration of the high temperature and radiation resistance required for aerospace applications [49–54] and the photovoltaic performances of SMPSCs can be enhanced by using SMPs with higher transparency [16] in other application scenarios. Furthermore, the efficiency of the SMPSCs can be improved by using AgNW/SMP composite electrode in flexible solar cell with high efficiency, like flexible perovskite solar cells [55–57].

The 3D AFM surface images of SMPI/AgNW/PEDOT:PSS, glass/ITO/PEDOT:PSS, SMPI/AgNW/PEDOT:PSS/P3HT:PCBM, and glass/ITO/PEDOT:PSS/P3HT:PCBM films are illustrated in Fig. 4, and the 2D AFM images are illustrated in Fig. S7. The corresponding RMS roughness is 1.13 nm, 1.63 nm, 4.15 nm, and 3.54 nm, respectively. The

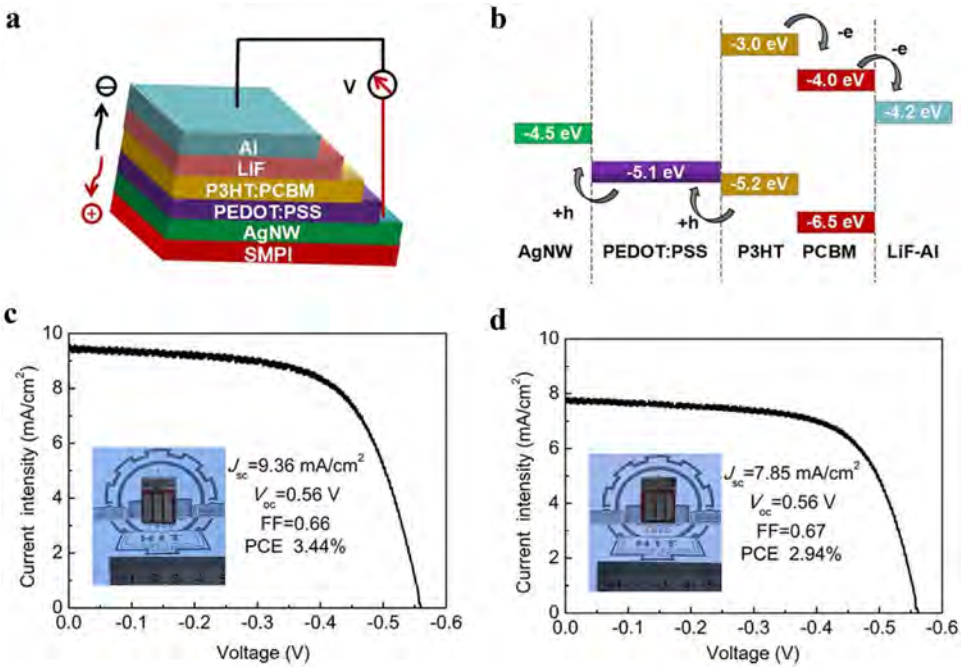

Fig. 3 **a** The complete layer stack of SMPSCs. **b** Band energy diagram for P3HT:PC61BM blend solar cells with SMPI/AgNW composite electrodes and Al electrodes. *J-V* characteristics for devices with ITO electrodes (**c**) and AgNW composite electrodes (**d**), and the inset photographs are the fabricated solar cells

results indicate that functional layers fabricated on the AgNW/SMPI electrode had similar surface quality to that fabricated on ITO/glass. The smooth surfaces are beneficial to reduce interface contact resistance and improve carrier flow. Furthermore, the grain-like composition of the surfaces guaranteed the good photovoltaic performances of solar cells due to the phase separation and the generation of macroscopic domains of a 1:1 blend of P3HT and PC61BM [58].

The performances of SMPSCs after different numbers of bending-recovery cycles and bending shape memory cycles were investigated. Figure 5a is the schematic of the shape memory cycle of SMPSCs. The SMPSC is firstly bent into the deformed shape at a temperature higher than the T_g of SMPI and then cooled while the deformed shape is maintained. The temporary shape can be fixed after the external mechanical load is removed. In the experiments, the shape memory cycle of SMPSCs was conducted inside the nitrogen-filled glove box. The SMPSC can recover to the original flat shape at 200 °C in 20 s (Movie S1).

From Fig. 5b, c, SMPSC demonstrated good flexibility and durability, and the photovoltaic performance of the SMPSC reduced slightly after 50 bending-recovery cycles. The *J-V* characteristics of SMPSCs before and after shape memory cycles are shown in Fig. 5d and the inset

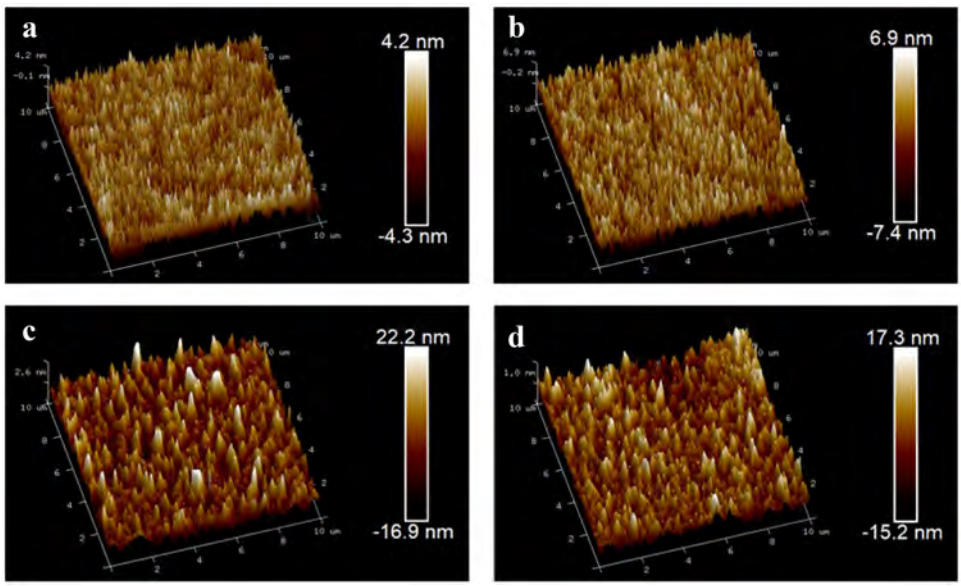

Fig. 4 3D surface images of **a** SMPI/AgNW/PEDOT:PSS after annealing at 120 °C for 20 min, **b** glass/ITO/PEDOT:PSS after annealing at 120 °C for 20 min, **c** SMPI/AgNW/PEDOT:PSS/P3HT:PCBM after annealing at 135 °C for 5 min, and **d** glass/ITO/PEDOT:PSS/P3HT:PCBM after annealing at 135 °C for 5 min

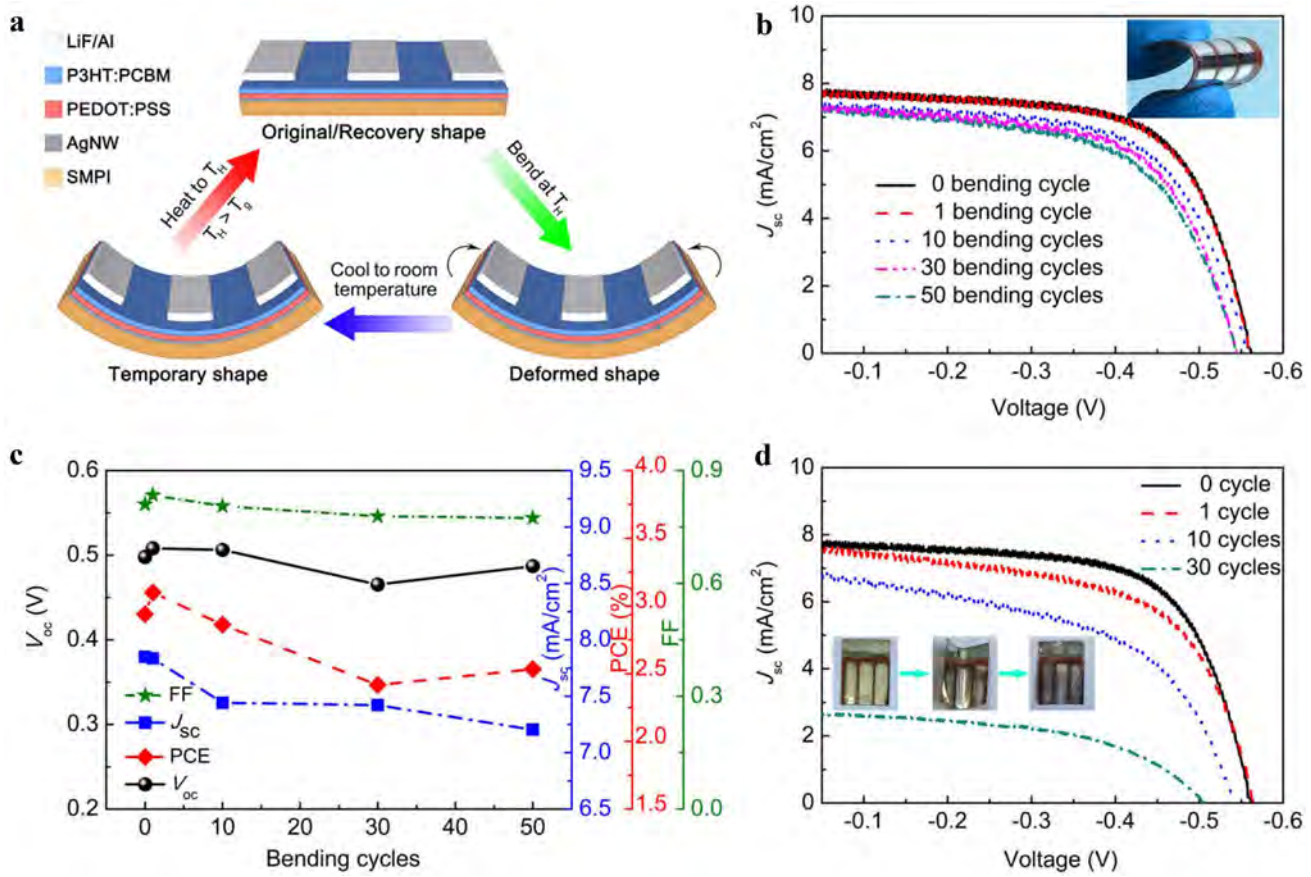

Fig. 5 **a** The bending shape memory cycles of SMPSCs. **b** *J-V* characteristics of SMPSCs after bending-recovery cycles, and **c** the effects of bending-recovery cycles on V_{oc}, J_{sc}, PCE, and FF. **d** *J-V* characteristics of SMPSCs after bending shape memory cycles, and the inset photographs are one shape memory cycle of real products

photographs shows the original state, deformed state, and recovery state of SMPSC in one shape memory cycle. The corresponding results of V_{oc}, J_{sc}, PCE, and FF are summarized in Table 2. The value of V_{oc} and FF was similar to the simulation results in reference [59]. However, the PCE of SMPSCs decreased from 2.94 to 2.00% after 10 shape memory cycles and dropped to 0.72% after 30 shape memory cycles. From Table 2, J_{sc} reduced most significantly after 30 shape memory cycles, which results from the decrease of electron–hole pairs. One reason is that the resistance of the AgNW/SMPI film increases by several times after 30 shape memory cycles, as shown in Fig. 2d. Another reason is that defects possibly generated in layers or interfaces [15] after multiple deformations at high temperature.

From the aforementioned results, the SMPSCs have the potential to be used in deployable solar arrays in the future. The shape memory property makes it possible to package or roll the ultra-large solar arrays based on SMPSC for reducing the space before launching and to actively deploy the solar array in space. The variable stiffness of SMP is also beneficial for the shape fixation after deployment. For the deployable solar arrays, limited shape memory cycles are usually required. In such case, the performance deterioration can be avoided, and the photovoltaic performance of SMPSCs has only slight reduction.

Table 2 Comparison of photovoltaic performances for devices after shape memory cycles

Substrates	R_s (Ω/□)	Shape memory cycle numbers	V_{oc} (V)	J_{sc} (mA/cm^2)	FF (%)	PCE (%)
AgNW/SMPI	~10	0	0.560	7.85	67	2.94
AgNW/SMPI	~10	1	0.566	7.58	61	2.61
AgNW/SMPI	~10	10	0.543	6.77	55	2.00
AgNW/SMPI	~10	30	0.506	2.66	54	0.72

4 Conclusion

In this paper, we demonstrate shape memory polymer solar cells with the structures of SMPI/AgNW/PEDOT:PSS/P3HT:PCBM/LiF/Al, of which AgNW/SMPI served as the transparent and conductive substrates. Due to the flexibility and durability of AgNW/SMPI composite electrode, SMPSCs were highly flexible and could be repetitively deformed with large strain. Moreover, owing to the shape memory property of the substrate, SMPSCs could be deformed into arbitrary shape and actively recover to the original shape upon heating. Though the PCE of SMPSC is lower than that of the control device fabricated on ITO/glass substrate, the photovoltaic performances of SMPSCs just had slight reduction after 50 bending-recovery cycles or few shape memory cycles. However, the photovoltaic performances deteriorated severely after large number of shape memory cycles. The SMPSCs have the potential to be used in deployable solar arrays in the future, and the transparent AgNW/SMPI composite electrodes may also be used in areas of sensors, medical probes, displays, and so on.

Supplementary information The online version contains supplementary material available at https://doi.org/10.1007/s42114-021-00263-8.

Funding This work was supported by the National Natural Science Foundation of China (Grant No. 11632005).

Availability of data and material Data are available from the authors upon reasonable request.

Declarations

Competing interests The authors declare no competing interests.

References

1. Liu Y, Du H, Liu L, Leng J (2014) Shape memory polymers and their composites in aerospace applications: a review. Smart Mater Struct 23:023001
2. Gao H, Lan X, Liu L, Xiao X, Liu Y, Leng J (2017) Study on performances of colorless and transparent shape memory polyimide film in space thermal cycling, atomic oxygen and ultraviolet irradiation environments. Smart Mater Struct 26:095001
3. Gao H, Xie F, Liu Y, Leng J (2018) Effects of γ-radiation on the performances of optically transparent shape memory polyimides with a low glass transition temperature. Polym Degrad Stab 156:245–251
4. Gall K, Yakacki CM, Liu Y, Shandas R, Willett N, Anseth KS (2005) Thermomechanics of the shape memory effect in polymers for biomedical applications. J Biomed Mater Res A 73:339–348
5. Huang WM, Yang B, An L, Li C, Chan YS (2005) Water-driven programmable polyurethane shape memory polymer: demonstration and mechanism. Appl Phys Lett 86:114105
6. Luo X, Mather PT (2010) Conductive shape memory nanocomposites for high speed electrical actuation. Soft Matter 6:2146–2149
7. Mohr R, Kratz K, Weigel T, Lucka-Gabor M, Moneke M, Lendlein A (2006) Initiation of shape-memory effect by inductive heating of magnetic nanoparticles in thermoplastic polymers. Proc Natl Acad Sci USA 103:3540–3545
8. Small W IV, Wilson TS, Benett WJ, Loge JM, Maitland DJ (2005) Laser-activated shape memory polymer intravascular thrombectomy device. Opt Express 13:8204–8213
9. Li W, Liu Y, Leng J (2015) Selectively actuated multi-shape memory effect of a polymer multicomposite. J Mater Chem A 3:24532–24539
10. Behl M, Lendlein A (2007) Shape-memory polymers. Mater Today 10:20–28
11. Wang W, Shen R, Cui H, Cui Z, Liu Y (2020) Two-stage reactive shape memory thiol-epoxy-acrylate system and application in 3D structure design. Adv Compos Hybrid Mater 3:41–48
12. Lai H, Shang Y, Cheng Z, Lv T, Zhang E, Zhang D, Wang J, Liu Y (2019) Control of tip nanostructure on superhydrophobic shape memory arrays toward reversibly adjusting water adhesion. Adv Compos Hybrid Mater 2:753–762
13. Reeder J, Kaltenbrunner M, Ware T, Arreaga-Salas D, Avendano-Bolivar A, Yokota T, Inoue Y, Sekino M, Voit W, Sekitani T, Someya T (2014) Mechanically adaptive organic transistors for implantable electronics. Adv Mater 26:4967–4973
14. Gao H, Li J, Zhang F, Liu Y, Leng J (2019) The research status and challenges of shape memory polymer-based flexible electronics. Mater Horiz 6:931–944
15. Avendano-Bolivar A, Ware T, Arreaga-Salas D, Simon D, Voit W (2013) Mechanical cycling stability of organic thin film transistors on shape memory polymers. Adv Mater 25:3095–3099
16. Yu Z, Zhang Q, Li L, Chen Q, Niu X, Liu J, Pei Q (2011) Highly flexible silver nanowire electrodes for shape-memory polymer light-emitting diodes. Adv Mater 23:664–668
17. Zhao W, Qian D, Zhang S, Li S, Inganäs O, Gao F, Hou J (2016) Fullerene-free polymer solar cells with over 11% efficiency and excellent thermal stability. Adv Mater 28:4734–4739
18. Li Z, Liu Y, Zhang K, Wang Z, Huang P, Li D, Zhou Y, Song B (2017) Chemical modification of n-type-material naphthalene diimide on ITO for efficient and stable inverted polymer solar cells. Langmuir 33:8679–8685
19. Gong X, Yang Z, Walters G, Comin R, Ning Z, Beauregard E, Adinolfi V, Voznyy O, Sargent EH (2016) Highly efficient quantum dot near-infrared light-emitting diodes. Nat Photonics 10:253–257
20. Jang J, Kitsomboonloha R, Swisher SL, Park ES, Kang H, Subramanian V (2013) transparent high-performance thin film transistors from solution-processed SnO_2/ZrO_2 gel-like precursors. Adv Mater 25:1042–1047
21. Miller MS, O'Kane JC, Niec A, Carmichael RS, Carmichael TB (2013) Silver nanowire/optical adhesive coatings as transparent electrodes for flexible electronics. ACS Appl Mater Interfaces 5:10165–10172
22. Gomez De Arco L, Zhang Y, Schlenker CW, Ryu K, Thompson ME, Zhou C (2010) Continuous, highly flexible, and transparent graphene films by chemical vapor deposition for organic photovoltaics. ACS Nano 4:2865–2873
23. Becerril HA, Stoltenberg RM, Tang ML, Roberts ME, Liu Z, Chen Y, Kim DH, Lee BL, Lee S, Bao Z (2010) Fabrication and evaluation of solution-processed reduced graphene oxide electrodes for p-and n-channel bottom-contact organic thin-film transistors. ACS Nano 4:6343–6352
24. Kim KS, Zhao Y, Jang H, Lee SY, Kim JM, Kim KS, Ahn JH, Kim P, Choi JY, Hong BH (2009) Large-scale pattern growth of graphene films for stretchable transparent electrodes. Nature 457:706–710
25. Nikolou M, Dyer AL, Steckler TT, Donoghue EP, Wu Z, Heston NC, Rinzler AG, Tanner DB, Reynolds JR (2009) Dual n-and

p-type dopable electrochromic devices employing transparent carbon nanotube electrodes. Chem Mater 21:5539–5547
26. Zhang M, Fang S, Zakhidov AA, Lee SB, Aliev AE, Williams CD, Atkinson KR, Baughman RH (2005) Strong, transparent, multifunctional, carbon nanotube sheets. Science 309:1215–1219
27. Li J, Hu L, Wang L, Zhou Y, Grüner G, Marks TJ (2006) Organic light-emitting diodes having carbon nanotube anodes. Nano Lett 6:2472–2477
28. Krebs FC (2009) All solution roll-to-roll processed polymer solar cells free from indium-tin-oxide and vacuum coating steps. Org Electron 10:761–768
29. Galagan Y, Rubingh JEJ, Andriessen R, Fan CC, Blom PW, Veenstra SC, Kroon JM (2011) ITO-free flexible organic solar cells with printed current collecting grids. Sol Energy Mater Sol Cells 95:1339–1343
30. Kang MG, Kim MS, Kim J, Guo LJ (2008) Organic solar cells using nanoimprinted transparent metal electrodes. Adv Mater 20:4408–4413
31. Ghosh DS, Chen TL, Mkhitaryan V, Pruneri V (2014) Ultrathin transparent conductive polyimide foil embedding silver nanowires. ACS Appl Mater Interfaces 6:20943–20948
32. Yu Z, Li L, Zhang Q, Hu W, Pei Q (2011) Silver nanowire-polymer composite electrodes for efficient polymer solar cells. Adv Mater 23:4453–4457
33. Schubert S, Kim YH, Menke T, Fischer A, Timmreck R, Müller-Meskamp L, Leo K (2013) Highly doped fullerene C60 thin films as transparent stand alone top electrode for organic solar cells. Sol Energy Mater Sol Cells 118:165–170
34. Gaynor W, Burkhard GF, McGehee MD, Peumans P (2011) Smooth nanowire/polymer composite transparent electrodes. Adv Mater 23:2905–2910
35. Chen TL, Ghosh DS, Mkhitaryan V, Pruneri V (2013) Hybrid transparent conductive film on flexible glass formed by hot-pressing graphene on a silver nanowire mesh. ACS Appl Mater Interfaces 5:11756–11761
36. Zou J, Yip H, Hau SK, Jen AK (2010) Metal grid/conducting polymer hybrid transparent electrode for inverted polymer solar cells. Appl Phys Lett 96:203301
37. Yang L, Zhang T, Zhou H, Price SC, Wiley BJ, You W (2011) Solution-processed flexible polymer solar cells with silver nanowire electrodes. ACS Appl Mater Interfaces 3:4075–4084
38. Lee J, Connor ST, Cui Y, Peumans P (2008) Solution-processed metal nanowire mesh transparent electrodes. Nano Lett 8:689–692
39. Liu CH, Yu X (2011) Silver nanowire-based transparent, flexible, and conductive thin film. Nanoscale Res Lett 6:75
40. Hu L, Kim HS, Lee J, Peumans P, Cui Y (2010) Scalable coating and properties of transparent, flexible, silver nanowire electrodes. ACS Nano 4:2955–2963
41. Scardaci V, Coull R, Lyons PE, Rickard D, Coleman JN (2011) Spray deposition of highly transparent, low-resistance networks of silver nanowires over large areas. Small 7:2621–2628
42. Akter T, Kim WS (2012) Reversibly stretchable transparent conductive coatings of spray-deposited silver nanowires. ACS Appl Mater Interfaces 4:1855–1859
43. Lee P, Lee J, Lee H, Yeo J, Hong S, Nam KH, Lee D, Lee SS, Ko SH (2012) Highly stretchable and highly conductive metal electrode by very long metal nanowire percolation network. Adv Mater 24:3326–3332
44. Kim Y, Ryu TI, Ok KH, Kwak MG, Park S, Park NG, Han CJ, Kim BS, Ko MJ, Son HJ, Kim JW (2015) Inverted layer-by-layer fabrication of an ultraflexible and transparent Ag nanowire/conductive polymer composite electrode for use in high-performance organic solar cells. Adv Funct Mater 25:4580–4589
45. Jiang Y, Xi J, Wu Z, Dong H, Zhao Z, Jiao B, Hou X (2015) Highly transparent, conductive, flexible resin films embedded with silver nanowires. Langmuir 31:4950–4957
46. Kong D, Li J, Guo A, Zhang X, Xiao X (2019) Self-healing high temperature shape memory polymer. Eur Polym J 120:109279
47. Kong D, Li J, Guo A, Yu J, Xiao X (2021) Smart polyimide with recovery stress at the level of high temperature shape memory alloys. Smart Mater Struct 30:035027
48. Kong D, Li J, Guo A, Xiao X (2021) High temperature electromagnetic shielding shape memory polymer composite. Chem Eng J 408:127365
49. Song P, Liu B, Qiu H, Shi X, Cao D, Gu J (2021) MXenes for polymer matrix electromagnetic interference shielding composites: A review. Compos Commun 24:100653
50. Ruan K, Shi X, Guo Y, Gu J (2020) Interfacial thermal resistance in thermally conductive polymer composites: a review. Compos Commun 22:100518
51. Zhao J, Zhang J, Wang L, Li J, Feng T, Fan J, Chen L, Gu J (2020) Superior wave-absorbing performances of silicone rubber composites via introducing covalently bonded SnO2@MWCNT absorbent with encapsulation structure. Compos Commun 22:100486
52. Shi X, Zhang R, Ruan K, Ma T, Guo Y, Gu J (2021) Improvement of thermal conductivities and simulation model for glass fabrics reinforced epoxy laminated composites via introducing hetero-structured BNN-30@BNNS fillers. J Mater Sci Technol 82:239–249
53. Han Y, Shi X, Wang S, Ruan K, Chuyao Lu, Guo Y, Junwei Gu (2021) Nest-like hetero-structured BNNS@SiCnws fillers and significant improvement on thermal conductivities of epoxy composites. Compos Part B Eng 210:108666
54. Yan H, Dai X, Ruan K, Zhang S, Shi X, Guo Y, Cai H, Gu J (2021) Flexible thermally conductive and electrically insulating silicone rubber composite films with BNNS@Al2O3 fillers. Adv Compos Hybrid Mater 4: 36-50
55. Li Y, Meng L, Yang YM, Xu G, Hong Z, Chen Q, You J, Li G, Yang Y, Li Y (2016) High-efficiency robust perovskite solar cells on ultrathin flexible substrates. Nat Commun 7:10214
56. Roldan-Carmona C, Malinkiewicz O, Soriano A, Espallargas GM, Garcia A, Reinecke P, Kroyer T, Dar MI, Nazeeruddine MK, Bolink HJ (2014) Flexible high efficiency perovskite solar cells. Energy Environ Sci 7:994–997
57. Jia C, Zhao X, Lai YH, Zhao J, Wang PC, Liou DS, Wang P, Liu Z, Zhang W, Chen W, Chu YH, Li J (2019) Highly flexible, robust, stable and high efficiency perovskite solar cells enabled by van der Waals epitaxy on mica substrate. Nano Energy 60:476–484
58. Wang C, Zhang X, Li M (2013) Effects of temperature on performance of organic solar cells based on P3HT/PCBM. Chin J Power Sources 37:1588–1590
59. Thompson BC, Fréchet JM (2008) Polymer-fullerene composite solar cells. Angew Chem Int Ed 47:58–77

Publisher's Note Springer Nature remains neutral with regard to jurisdictional claims in published maps and institutional affiliations.